CFD simulation of the aerodynamic sealing of plane jets

J. Dias[1], A. Gogotsi[2] and J.C. Viegas[1]

[1]*Laboratório Nacional de Engenharia Civil, Av. do Brasil 101, 1700-066 Lisboa, Portugal*
[2]*Material Research Centre, Kiev, Ukraine*
Corresponding Author:J. Dias

Abstract: Controlling air quality is of the utmost importance within today's buildings. Vertical air curtains are often used to separate two different climatic zones in order to reduce heat transfer. This research work proposes an air curtain aimed to ensure a proper separation between two zones, a clean one and a contaminated one, which is to be used together with an air extraction from the "contaminated" compartment. A CFD parametric study was carried out in order to assess the optimal parameters for achieving the aerodynamic sealing of the air curtain. The software OpenFOAMwas used to carry out the simulations. This paper presents the numerical validation of the computational fluid dynamics model for contaminant control applications and the final simulation results. Furthermore, it refers to the test results obtained in the framework of previous research, which were obtained in both small scale and full size testing, and demonstrates that the simulation results are coherent with the experiments. This research work shows that, when properly implemented, the air curtains provide the adequate aerodynamic sealing to maintain the air contaminants within the "contaminated" compartment. The appropriate performance can be obtained for nozzle speeds as low as 1 m/s and for a nozzle thickness of 10 mm. The best performance is obtained when the extraction flowrate of the "contaminated" compartment corresponds to the total flowrate entrained by the air curtain from the "non-contaminated" side.

**Keywords:** Plane jets; Contaminant control; Air curtain; OpenFOAM.

I. INTRODUCTION

Air curtains are currently used to separate different environment zones. The main objectives of the air curtains are to reduce or control the heat and mass transfer and to reduce the spreading of airborne pollutants between zones. Its primary application occurs when the physical barriers are unacceptable for several reasons, either momentarily or permanently. In this framework, air curtains have been employed for several purposes such as: HVAC (Heating, Ventilation and Air Conditioning) [1-3], smoke control in passageways [4, 5], and airborne pollutant and biological control [6-8].

This study is developed within the framework of the Nanoguard2ar project (European Union's Horizon 2020 research and innovation programme under the Marie Sklodowska-Curie grant agreement N 690968). Its main goals are to develop, design, test, validate, and demonstrate an innovative nanomaterial-based 'microbial free' engineering solution, to ensure indoor air quality in buildings. To achieve this, an advanced oxidation process will be employed to clean the air extracted from the contaminated compartment (or to clean the external air before supplying it to the non-contaminated compartment), in conjunction with the use of air curtains, with a view to ensure a proper separation between the spaces that are to be kept without cross contamination. Therefore, the purpose of this study is to define the plane jet characteristics that make possible to achieve the best aerodynamic sealing of the air curtain, by ensuring low exhaust flow rates from the contaminated compartment (or supplying flow rates to the non-contaminated compartment), and ultimately reducing the air treatment costs. This research encompasses three phases, namely: (i) small-scale experiments using water as the work fluid; (ii) computational fluid dynamics (CFD) simulations to verify if the small-scale test results are applicable to full size air curtains; and (iii) full size air curtain experiments. The results of the first phase were presented by Viegas, Oliveira and Aelenei [9]. This paper describes the research carried out in the second phase.

The plane jet induces shear stress between the airflow and the stagnant ambient air, which eventually causes air entrainment. The turbulent structures promote the air mass transport from both sides into the jet (from "contaminated" and "non-contaminated" compartments) and the rejection of the contaminated jet flow to the clean compartment (e.g., when the downward jet impinges the floor) corresponds to the loss of aerodynamic sealing of the air curtain (loss of containment of the pollutants). As the entrainment increases with the volume flow rate at the air curtain nozzle, the usual application of this technology, with a view to maintain the "non-contaminated" compartment free from airborne pollutants (microorganisms, bacteria, fungus, particles), uses

low jet velocities to achieve a nearly laminar flow. An extraction at the "contaminated" side or at the tip of the jet is necessary to avoid the dispersion of the jet flow into the "non-contaminated" compartment (Figure 1a). Reversely, this objective may also be attained if "clean" air is supplied to the "non-contaminated" compartment (Figure 1b). The treatment of the "clean" air before supplying it to the "non-contaminated" compartment or the treatment of the "dirty" air removed from the "contaminated" compartment before releasing it to the environment are expensive procedures. Therefore, it is relevant to find a technical solution for achieving a zone separation that minimizes flow rate requirements.
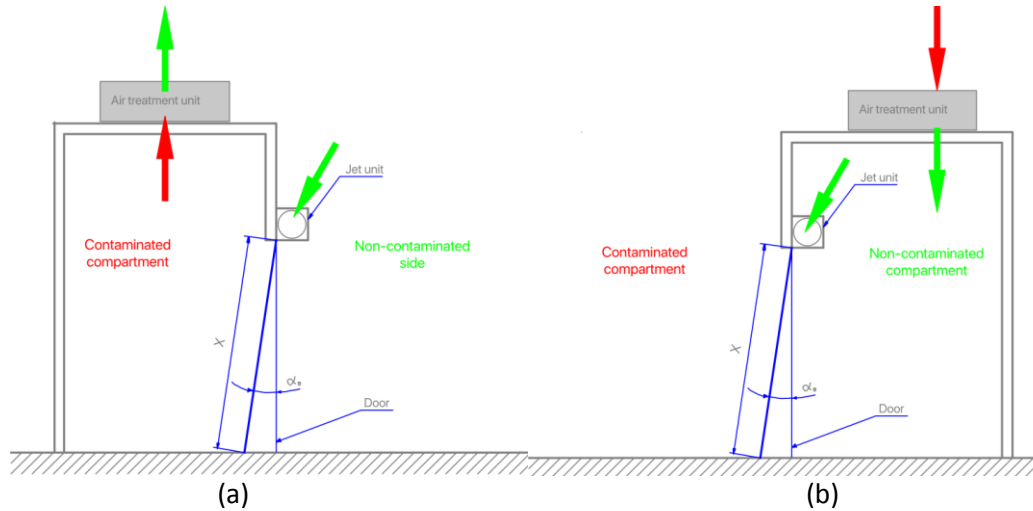
Figure 1: Strategies for containing a contaminant within a compartment (a) and for protecting a clean room (b).

Even though for an undisturbed environment (e.g., isothermal flow) the best solution is just to provide a very small uniform horizontal air stream through the opening, in the practice, some disturbances are likely to occur (e.g., temperature differences, air drafts due to the wind, people crossing the opening), which require the use of an air curtain to improve the aerodynamic sealing of the opening. For this purpose, the most effective air curtain is the one that provides an acceptable aerodynamic sealing performance for airborne contaminants, by minimizing the exhaust (or supply) flow rate, when exposed to disturbances.

In the air curtain applications at door height openings, the flow is actually characterized by a transition or turbulent regimen. The overall jet flow rate is reduced if the jet velocity is decreased; and hence, the use of lower jet velocities is also a strategy that can be adopted to reduce the jet flow rate rejected to the 'non-contaminated' compartment. Nevertheless, the vertical downward air curtains must be properly designed so as to avoid splitting the jet flow at the floor impingement zone, and consequently losing the air curtain aerodynamic sealing. However, with low air curtain speeds, when people walk through the door, the air curtain reconstitution time is longer, which could increment pollutant leakage through the air curtain. Using air curtains in a transition regimen (rather than in a laminar regimen) can minimize this problem.

Hayes and Stoecker [10–12] studied the aerodynamic sealing performance of vertical air curtains under both isothermal and non-isothermal conditions. Hayes [10] developed the deflection modulus (Dm), which is indicative of the deflection of the air curtain jet and expresses the ratio of the outlet momentum to the transverse forces on the jet [12]. They defined [11] the operation condition, in which the air curtain jet reaches the floor, as the 'optimum condition' and the other operation conditions, in which the air curtain jet does not reach the floor, as 'break-through conditions'. The latter can be further divided into 'inflow breakthrough condition', in which the air curtain flow is curved inwards and does not reach the floor, and 'outflow breakthrough condition', in which the air curtain flow is curved outwards and does not reach the floor [13, 14]. In our research, the ideal condition corresponds to the limit between the optimum condition and the inflow breakthrough condition, when having Figure 1a as reference. Indeed, in this condition, the contaminant mixed up in the jet flow is not released to the outside of the compartment.

There are several applications of this concept that are aimed to avoid contaminant spreading, such as: in operating rooms [7,15–20], for tobacco smoke control [21,22], for protection of art works in museums and of cultural heritage [23,24], and in open refrigerated display cabinets [25,26]. Several studies about air curtain efficiency have been conducted on these applications. However, there is no systematic approach to the contaminant aerodynamic sealing in the transition between the optimum condition and the 'inflow breakthrough condition'. The studies on the application of air curtains have been based on experiments [13,27–30], on CFD models [24,30,31], and on semi-analytical models [14,32].

Santoli, Cumo, and Mariotti [24] presented a numerical and experimental study on a cultural heritage building, using an air jet with speeds between 4 and 5 m/s, to create a physical barrier to the flow. They concluded that the ventilation system has efficiencies of 70–75%. However, the parameters that allow maximizing the efficiency of the air curtain were not analyzed in this study.

Zhai and Osborne [15] presented a numerical and experimental study, in which they concluded that there is no correlation between the laminar flow diffuser, the air curtain flow rate, and the concentration of contaminants. It was observed that it was preferable to use one-way diffusers rather than air curtains with high jet velocities. However, this did not demonstrate the existing relation between diffuser and air curtain flow rates.

Wang and Zhong [31] developed an approach to determine the infiltration and the exfiltration characteristics of building entrance equipped with an air curtain. A detailed parametric study for different ambient temperatures, pressure differences across the air curtain and different door usage frequencies was conducted by computational fluid dynamics simulations with the ANSYS FLUENT commercial software package [33]. They noticed that many previous studies used CFD with the standard k−ε turbulence model to simulate air curtains. Thus, they carried out CFD steady state simulations based on that turbulence model. The calculated air infiltration rates were then correlated to the pressure differences across the air curtain. The numerical approach was first verified by comparing the correlations obtained for the building entrance without an air curtain with the data published in the literature. New infiltration/exfiltration correlations of the modeled air curtain were then developed as a function of pressure difference, flow coefficient, and flow modifier. Compared to the single door without an air curtain and the door with vestibule, the air curtain was found to significantly reduce the infiltration, especially for the mild ranges of pressure differences.

These works clearly stress the relevance of the pressure difference between the interior and the exterior of the compartment, which is due to several factors, such as the buoyancy effect, the head loss of the flow through the opening, and many other factors including the wind effect and the indoor system operation; however, in the absence of the buoyancy effect, this pressure difference through the opening protected by the air curtain is related with the head loss of the flow through the opening protected by the air curtain. As the head loss is dependent on the characteristics of the opening [35], in our research, we considered that the average velocity of the flow across the door $(\overline{(u_a)})$ is the variable of reference.

In the mentioned works, no clear correlation was established between the inlet flow rate (flow entering the door opening), the velocity at the jet nozzle and the aerodynamic sealing of the air curtain. As there is usually no concern in reducing the exhaust flow from the contaminated compartment (or the supply flow to the non-contaminated compartment), in order to increase the effectiveness of the curtain and to reduce the air cleaning costs, both the air velocities and the corresponding Reynolds numbers in these works are quite high when compared with those reported in our research work. Therefore, to the best knowledge of the authors of this work, our study, which is focused on low velocity jets and low extraction flow rates, constitutes an added value to research in the field.

Therefore, the main purpose of the research presented hereafter is to access the possibility of using low velocity plane jets associated to a small extraction rate from the contaminated side to obtain aerodynamic sealing at the air curtain.

As in the research presented by Qi et al. [30], in our research both a small-scale model and full size CFD simulations were carried out for studying the aerodynamic sealing performance of plane jets as regards pollutant containment. In a previous research [4, 37], the extreme condition of the curtain exposed to a high buoyancy action was studied, whereas the research study presented here was focused on the opposed extreme condition of non-buoyant flow. In a previous paper [9], the research presented employed a methodology that included: (i) small-scale tests on water models to ensure that the contamination did not pass through the air curtain, and (ii) an analytical development integrating the main physical characteristics of plane jets. In this paper, CFD simulations were carried out to demonstrate that the results obtained in small-scale water testing are applicable to full size air curtains. This work is expected to continue in the future by applying these principles to full size air curtain experiments.

In the solution developed, the airflow was extracted from the contaminated compartment to reduce the curtain airflow rejected to the exterior of the compartment. In a previous paper [9], it was possible to determine the minimum exhaust flow necessary to ensure the aerodynamic sealing of the air curtain. A simplified analytical model was presented with a view to discuss the variables that can influence the performance of the plane jets under a turbulent transition regimen.

In this paper, the validation of the CFD model is firstly presented (based on the OpenFOAM software package) and, then, the model is used to investigate the aerodynamic sealing performance of the air curtain under the influence of different nozzle velocities (1.0 m/s and 0.5 m/s), of different curtain angle (the range [10°; 0°] was investigated), of different nozzle thicknesses (from 5 mm to 25 mm) and under variable exhaust flow rate from the "contaminated" compartment (Figure 1a). Finally, the results from a previous research (small

scaleisothermal flow [9], small scale buoyant flow [4] and full-size buoyant flow [37]) are analyzed together with the ones obtained with the simulations presented here to show the coherence of the results.

II. METHODS

a. Numerical Models

In this work, the aerodynamic sealing performance of an air curtain is carried out through CFD analysis using the OpenFOAM code. The contaminant modelingis done by a passive scalar equation. A passive scalar is a quantity directly related to a fluid and which does not influence its properties that are important from the point of view of the fluid dynamics [36]. This method considers that the passive scalar does not react. The numerical validation of the plane jet against the analytical solution and the validation of the model against experimental full scale data are also presented. The parameters of the air curtain and their influence on the contaminant flow are analyzed.

The OpenFOAM code includes several generic solvers for each class of applications and libraries that can be added in order to develop a specific solver for each problem. These solvers applied to computational fluid dynamics use the finite volume method to solve the governing equations of thermodynamics and fluid dynamics. In this work, two steady state solvers are used, depending on whether the energy equation is modeled or not.

In a first step, the *buoyantSimpleFoam* solver, that solves the energy equation, was used to validate the numerical model against full scale experimental data (obtained from a previous research [37]), which consisted of a fire experiment using an air curtain to retain the smoke. In a second step, the *simpleFoam* solver (isothermal conditions) was used, including a passive scalar transport equation, with a view to model the effect of the contaminant (air pollution concentration) on the flow. The passive scalar allows studying the different parameters that assure the aerodynamic sealing efficiency of the air curtain.

The *buoyantSimpleFoam*, which assumes an incompressible and steady state condition, was adopted to model the effect of the buoyancy. This model, still under development, does not model combustion, radiation and particle concentration. Thus, a simplified approach was used, which was based on the characterization of combustion as a volumetric heat source. Modeling with a volumetric heat source leads to the calculation of the temperature field by modifying the source term in the energy equation, without taking into account either the combustion modelling (combustion product formation and chemical kinetics) or the heat transmission by radiation.

The convective heat output was evaluated on the basis of the exhaust smoke temperature [37]. Thus, it was observed that the convective heat release rate value, in the experiments corresponding to the simulations carried out, reaches about 40% of the total heat released. The volume associated with the heat source, representative of the volume occupied by the flame, was estimated based on the height of the flame (L_f); the latter being evaluated by the empirical equation that correlates the flame height with the convective heat released rate and with the diameter [38].

$$L_f = -1,02D + 0,235\dot{Q}^{2/5} \qquad (1)$$

where D is the diameter of the pool fire (with the value of 720 mm in those experiments) and $\dot{Q}$ is the total heat release rate. A plume height of 1.6 m was estimated.

The standard k-ε turbulence model, with the typical default constants, was used [39]. This model has been extensively and successfully applied to fire scenarios and recirculation flows. Despite it being a simplistic model, when compared to other models, it is highly recommended in terms of computing time.

The sub-relaxation coefficients of variables were set at 0.7, except for the passive scalar variable that was set at 1 (no relaxation). The initial turbulence conditions, for the turbulence kinetic energy (k) and dissipation rate (ε) parameters, were computed from equations $k = \frac{3}{2}Iu^2$ and $\varepsilon = C_\mu^{3/4}\frac{k^{3/2}}{l}$, where C_μ is an empirical constant specified in the turbulence model (the value 0.09 was considered), u is the jet nozzle velocity, and I is a turbulence intensity of 1%. From the equations above, the initial values of parameters k and ε were computed with the value of 0.01.

In order to model the effect of the contaminant/pollutant, on the area above the door, the boundary conditions were applied, with an "inflow type condition", having a passive scalar inlet condition with value 1 (representing the maximum concentration of contaminant) and being subject to contaminant inlet velocity of 0.05 m/s. This contaminant flow rate, although low and inducing a minimal disturbance in the flow, was taken into account in the exhaust flow rate.

A steady-state model was used to establish and validate initial parameters, such as boundary conditions, turbulence models, and numerical schemes. A numerical scheme of first-order upwind was used for the upstream differences. The coupling between pressure and velocity, available for a steady-state flow, is

performed by an iterative method with the SIMPLE (Semi-Implicit Method for Pressure-Linked Equations) algorithm [40]. The numerical schemes that transform the algebraic variables used are the Preconditioned Conjugate Gradient (PCG) and the PBiCG (Preconditioned Bi-Conjugate Gradient), for both the pressure and the remaining variables (U, h, k, ε), respectively. The solution convergence was established on basis of the following criteria:

a) residuals less than 10^{-6};
b) temperature profile in the several columns remaining constant throughout the successive iterations;
c) exhaust mass flow remaining constant throughout the successive iterations and a condition showing that the exhaust temperature remains constant; based on these criteria, it was verified that the simulation always converged below 50000 iterations.

In the wall-type boundary conditions, a non-slip condition was applied, by defining velocities at zero and adiabatic walls for calculating the temperature, i.e., by establishing a zero temperature gradient. In the volumetric heat source, a constant release heat rate was imposed, which was uniformly distributed throughout the fire volume.

In order to validate the numerical model, three validation procedures were performed: (i) plane jet simulation by comparison with the analytical solution; (ii) inactive air curtain simulation; and (iii) active air curtain simulation against full scale experimental data. In the simulations with and without an active air curtain, experiments were carried out with a similar convective power. With this validation, it is possible to assure the feasibility of the solver in modeling the dynamic behavior of the turbulent flow with the jet and exhaust systems.

The general equation of the passive scalar transport in steady state is written by equation (2). A comprehensive review of the literature on passive scalars and turbulence is given by Warhaft [41].

$$\nabla \cdot (\emptyset \, s) - \nabla \cdot ((\mu + \mu_t)\nabla s) = 0 \qquad (2)$$

Where s is the passive scalar, μ is a laminar viscosity and μt a turbulent viscosity.

b. Model Validation

Firstly, the downward vertical plane jet was validated under an isothermal regime in a two dimensional calculation domain of dimensions 2 m x 2 m, which was discretized through a uniform Cartesian mesh. Three simulations were performed for nozzle velocities, U0, of 1.0 m/s, 19.9 m/s (both with a 0° slope of the jet relatively to the plane) and of 19.9 m/s with an angle of 22°. A 25 mm nozzle thickness was adopted in all cases. The profiles of the numerical results were systematically compared with the free plane jet analytical solution Eq. (3) [42]:

Where U(x,y) is the longitudinal velocity of the jet, b0 is the nozzle thickness, U0 is the velocity of the jet at the nozzle, x is the longitudinal coordinate of the jet and y is its transversal coordinate. This equation represents the average (temporal) longitudinal component of the velocity field while the results of the simulations correspond to the magnitude of the velocity vector and, hence, they include the transverse component to the flow caused by the entrainment of air.

Figure 2 shows the velocity profile for the three simulations, by respectively considering jet velocities of 1.0 m/s (images a) to c)), 19.9 m/s (images d) to f)) and 19.9 m/s, with a slope of 22° (images g) to i)) for the three different sections as follows: at 0.5 m, 1.0 m and 1.5 m from the jet nozzle. It can be seen that the velocity profile in the sections near the jet nozzle is very conservative resulting in speeds higher than the analytical solution. This effect, which occurs in areas near the nozzle, becomes less important both in high velocity jet simulations and in inclined free jet simulations. It is observed that with the increase in the distance to the origin, the velocity profile agrees with the analytical solution. As the most relevant part of the jet for this research is the zone near the door sill, where the aerodynamic sealing may be lost, we consider that these validation results are acceptable.

Further validation of the CFD modeling was made using experimental results obtained in a previous research project on the use of air curtains to avoid smoke flow (from a fire) through openings (like doors) [37]. It has been considered that a validation for a non-isothermal case is more general and enables the use of the validated application for the particular case of an isothermal flow.

In a previous research [37], in order to assess the aerodynamic sealing (smoke tightness) of an opened door protected by an air curtain in a compartment, a full-scale experimental model was built inside a hangar (see Figure 3). The compartment had the dimensions of 5.0 m x 4.0 m and was 2.8 m high. The walls consisted of a double 10 mm thick gypsum board and of a 50 mm insulation layer. It also had an opening to the outside (door) of a 0.9 m width and a 2.0 m height. The compartment was equipped with an exhaust fan (containing a speed regulator) having a flow rate of up to 4.25 m3/s. The exhaust opening was located at the top of the wall opposite to the door and had the dimensions of 0.625 m x 0.535 m. The exhaust flow rate from the compartment was measured by an anemometer at the exhaust opening and was used to calibrate the frequency imposed on the drive, which was used as reference for further tests. A thermocouple was placed at the fan intake and another

thermocouple was placed at the compartment exhaust opening. These thermocouples made it possible to continuously evaluate the cooling of the smoke in the connecting duct to the fan, so as to be able to correct the total flow rate effectively exhausted from the compartment.
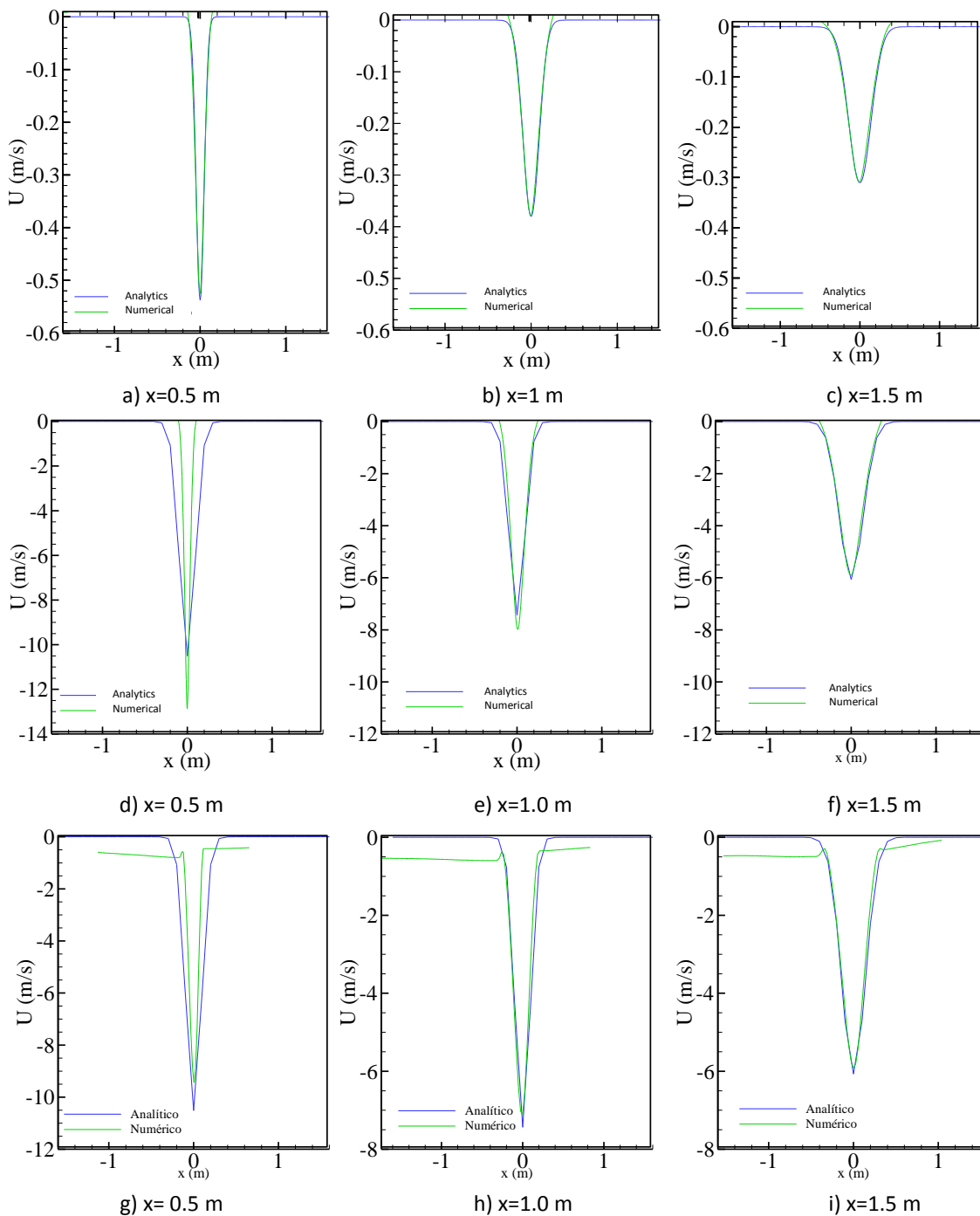
Figure 2: Comparison of the velocity profiles with the analytical solution: vertical jet with $U_0=1,0$ m/s - images a) to c); vertical jet with $U_0=19,9$ m/s- images d) to f); inclined jet with $U_0=19,9$ m/s and an angle of 22°- lines g) to i).

The fan prototype that generated the air curtain was placed on the door lintel edge outside the compartment in the downward vertical jet configuration. The jet is wider that the door in order to avoid any leakage between the jet and the door lateral walls. The air flow velocity in the air curtain was controlled by adjusting the frequency in a variable speed drive; the speed being continuously measured by a hot wire anemometer located at the jet nozzle. The measurements of this anemometer were correlated with the average jet velocity by previous calibrations. The curtain speed at the source varied (for the various experiments)

between 12.6 m/s and 20.8 m/s. The heat source consisted of a gasoline pool fire, with a 720 mm diameter. In order to assess the heat release rate, gasoline consumption was assessed by the mass loss with a calibrated load cell. This method of measurement of the heat release rate was calibrated by analysing the oxygen content in the combustion products ("oxygen consumption method"). The heat source was located at point (2.115 m; 3.250 m) of the X0Z plane (see Figure 3). Inside the compartment, 12 K type thermocouples were installed on the walls and 60 J type thermocouples were arranged in three vertical columns. A fourth column was placed next to the door, outside the jet, which was designed to assess the aerodynamic sealing of the door. In each test, the curtain flow rate and the exhaust flow rate from the compartment were reduced until the aerodynamic sealing limit was reached in the curtain.
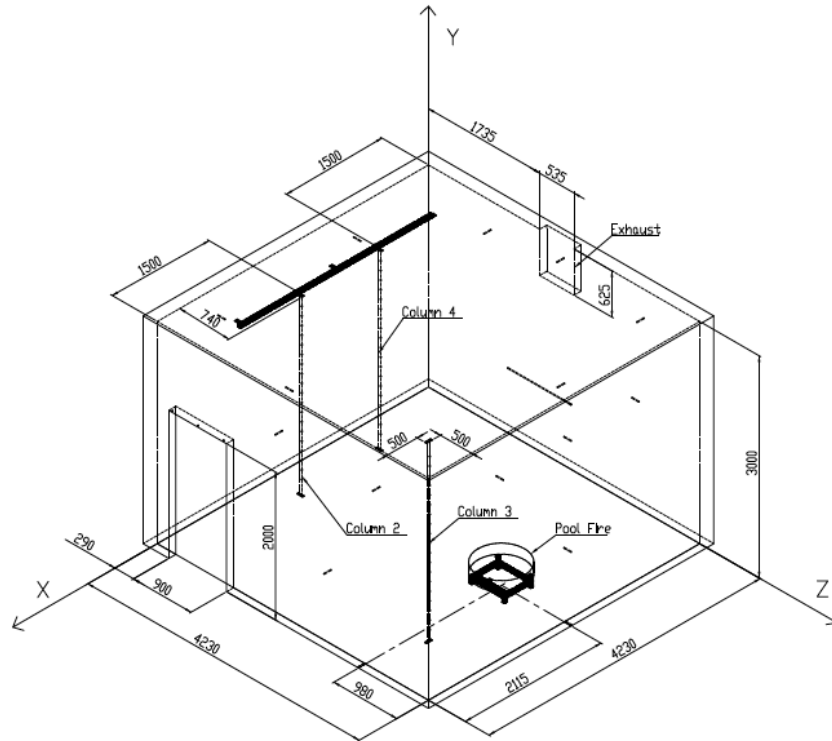

Figure 3: Test compartment.

The tests confirmed the potential of the downward vertical air jet, together with the smoke extraction from the compartment, to avoid the smoke flow through the air curtain. In addition, three experiments were carried out with an inactive air curtain to obtain reference conditions of the indoor environment in the fire scenario.

In Figure 4 (left), with the air curtain inactive, it is possible to observe a considerable smoke flowrate through the door and in the same Figure 4 (right), but with the air curtain active (and keeping the other conditions unchanged), it is possible to observe the sealing potential of the air curtain.
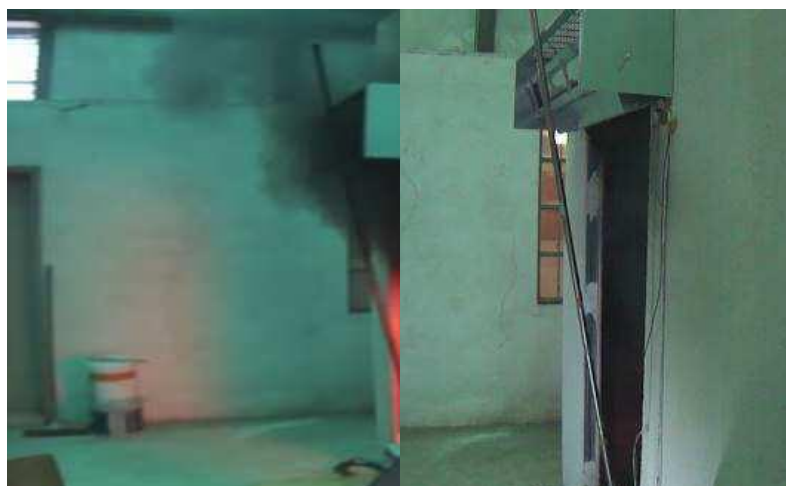
Figure 4: Experiment with an inactive air curtain (left) and an active air curtain (right).

The validation of the inactive air curtain was performed to verify the performance of the numerical model in describing the reference conditions of the indoor environment in the fire scenario. To evaluate the independence of the mesh solution, simulations were performed with three types of 3D structured meshes, having 400340 (mesh 01), 427740 (mesh 02) and 705680 (mesh 03) elements, respectively. In the case of mesh 02 zone refinement was performed in order to optimize the number of elements. Thus, due to the local refinement, the number of elements in the door area and in the zone of the volumetric heat source was increased in relation to mesh 01. It was generally observed that the temperature profile of the numerical results was similar to the measured profiles (Figure 5). In the thermocouple column at the door, this discrepancy was greater, probably due to the effect of the direct radiation heating of thermocouples at lower height, which overlook the heat source because they are outside the smoke layer. Additionally, it was observed that the temperature profiles between mesh 02 and mesh 03 were similar (Figure 5), which demonstrates the independence of the solution from these meshes.
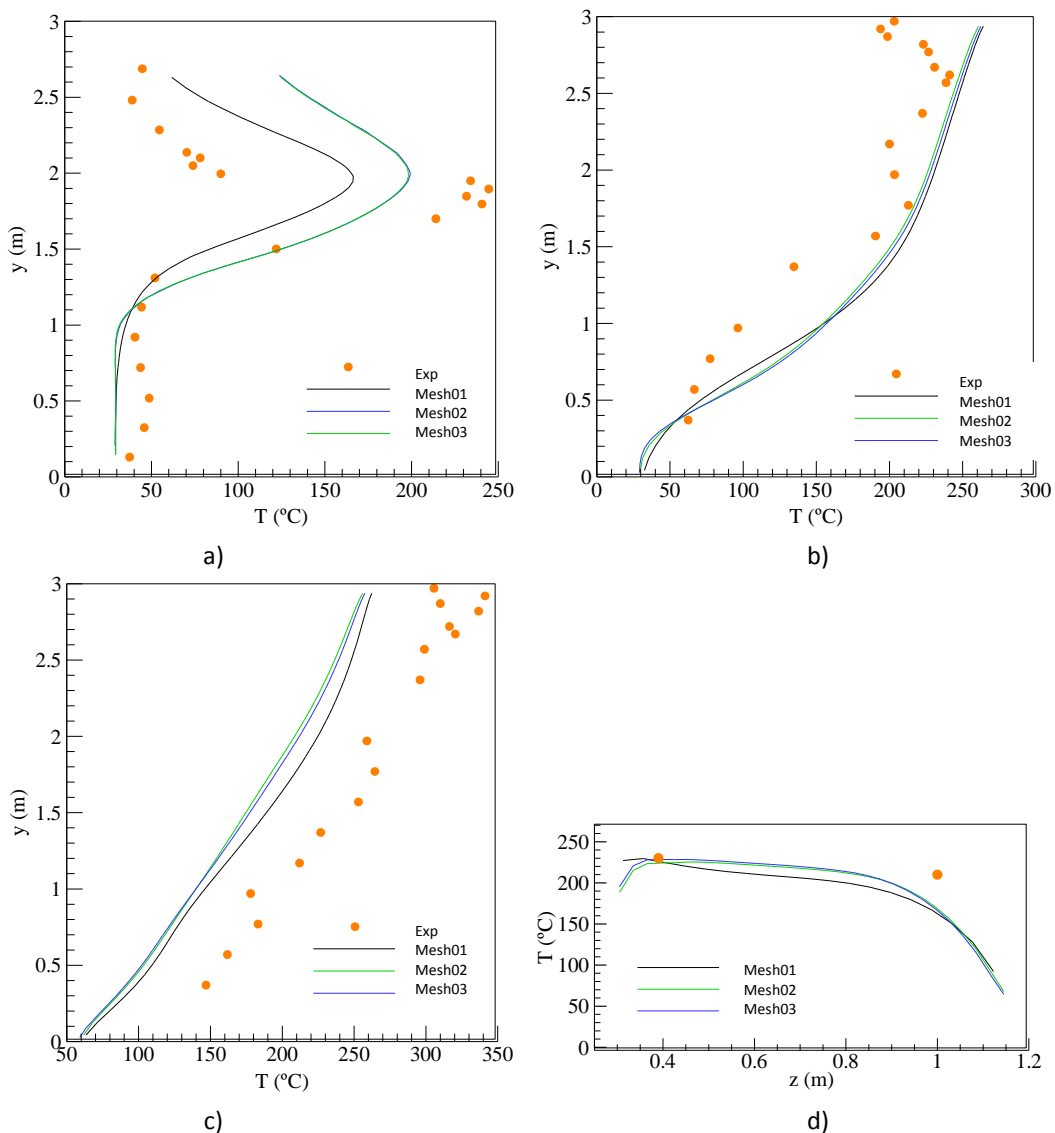
Figure 5: Temperature profiles with an inactive air curtain: a) column 1; b) column 2; c) column 3; d) Thermocouples at the top of the door.

The third validation focused on the performance and application of air curtains to ensure the aerodynamic sealing (smoke tightness). The discretization used for the simulation with an active air curtain was performed based on mesh 02, referred to in the previous validation, and based on the 2D mesh used in the validation of the plane jet.

Smoke tightness at the opening can be obtained by optimizing the exhaust flow rate and using a plane jet of the clean air curtain. Figure 6 presents a comparison between the temperature profiles of the numerical simulations and the measured data. It is observed that the numerical results have the same behaviour as the experimentally measured temperature profiles. Nevertheless, it was found that the simulated temperature field in the zone below the smoke layer, particularly in the thermocouple column at the door, was significantly less than the measured values. This discrepancy is due to the fact that the radiation was not simulated. Nonetheless, this difference is not so pronounced in the range of temperatures near the ceiling due to the opacity of the smoke, on which the effect of the direct radiation from fire is not so intense. It is observed that the use of the air curtain impairs the thermal stratification. However, in Figure 7, it can be seen that the thermal stratification can still persist, as in the experimental case. It was concluded that the model correctly simulates the convective flow at the door and is able to evaluate the aerodynamic sealing (smoke tightness). In order to improve the simulation results, a combustion model (combustion product formation and chemical kinetics) and a radiation model must be implemented, but these models are not necessary for the isothermal simulations presented later on.

III.   SIMULATION RESULTS

Several numerical simulations, using OpenFoam computer code, were done in order to study the efficiency and to analyse the air curtain parameters, in association with an exhaust system. A sensitivity analysis was carried out relating to several parameters, namely: jet nozzle thickness, jet nozzle velocity, jet angle and exhaust flow rate. The nozzle velocities studied corresponded to 0.5 m/s 1.0 m/s. The jet angles studied corresponded to 0º, 5º and 10º. The influence of nozzle thicknesses of 5 mm, 10 mm and 25 mm, respectively, was also studied.


a)

b)

c)
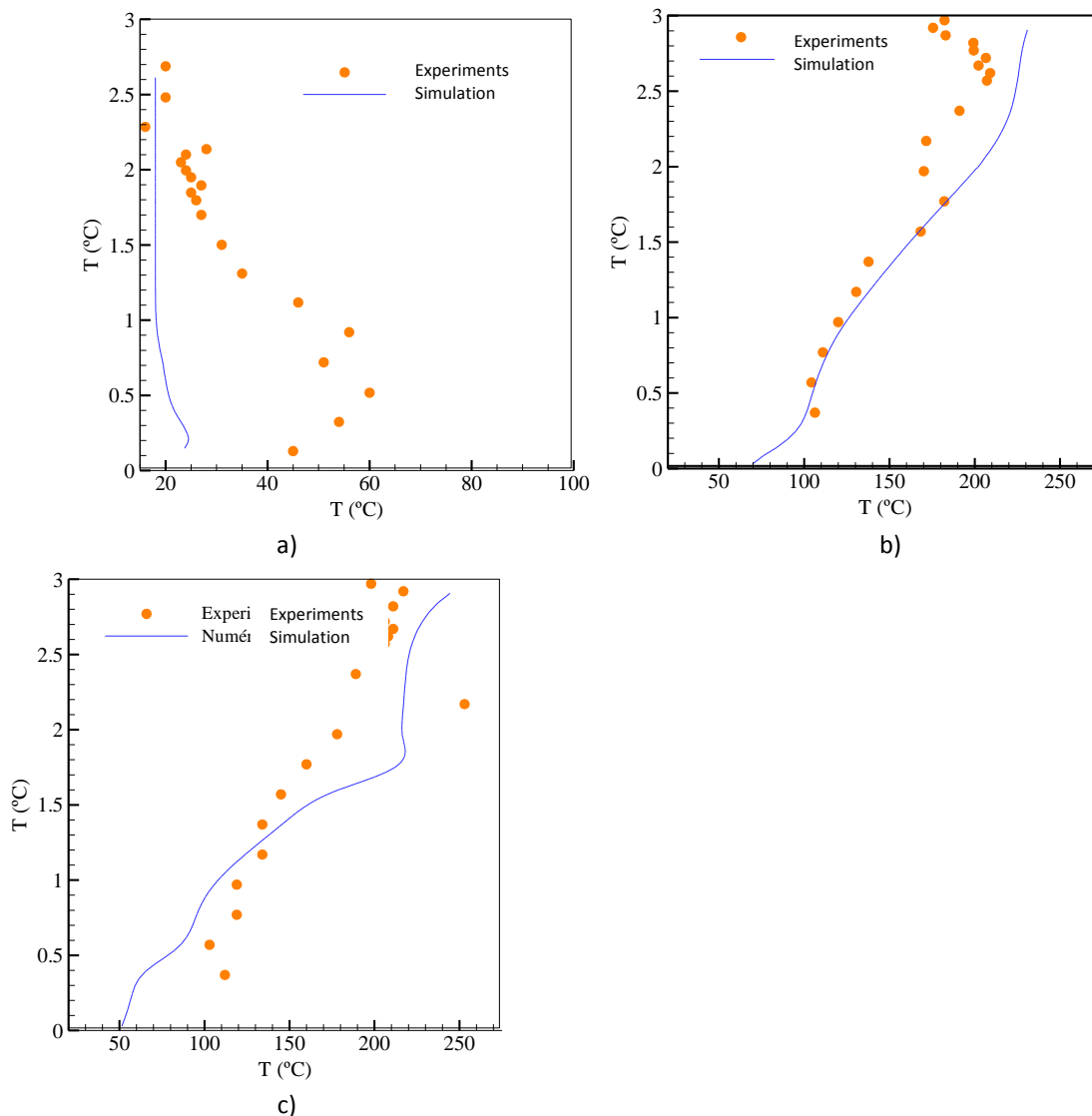
Figure 6: Temperature profile with the active air curtain: a) column 1; b) column 2; c) column 3.

Every simulation was performed with the same number of mesh elements at the nozzle (five elements at the nozzle thickness). Although the jet thickness was varying, to maintain the same aspect ratio of elements, the number of elements in the x direction was increased. Therefore, the total number of mesh elements increased when the nozzle thickness decreased. The total number of elements for jet thicknesses of 25 mm, 10 mm and 5 mm was 81000, 1103150 and 1735400, respectively.

Equation (4) expresses the total flow rate incorporated in the jet from the outside [9]. The term $\left[0.22\left(\frac{2x}{b_0}\right)^{0.5}\overline{u_0}wb_0\right]$ corresponds to half of the jet flow rate (that encompasses half of the nozzle flow rate and the outside "non-contaminated" air entrained by the jet). The term $[0.5\,\overline{u_0}wb_0]$ corresponds to half of the jet nozzle flow rate, which is supplied from the external "non-contaminated" air. The parameter K included in equation (4) must be assessed in this research with a view to obtain the desired restriction to the transport of contaminants through the air curtain.

$$\dot{V}_{exaust} = K\left[0.22\left(\frac{2x}{b_0}\right)^{0.5} + 0.5\right]\overline{u_0}wb_0 \tag{4}$$
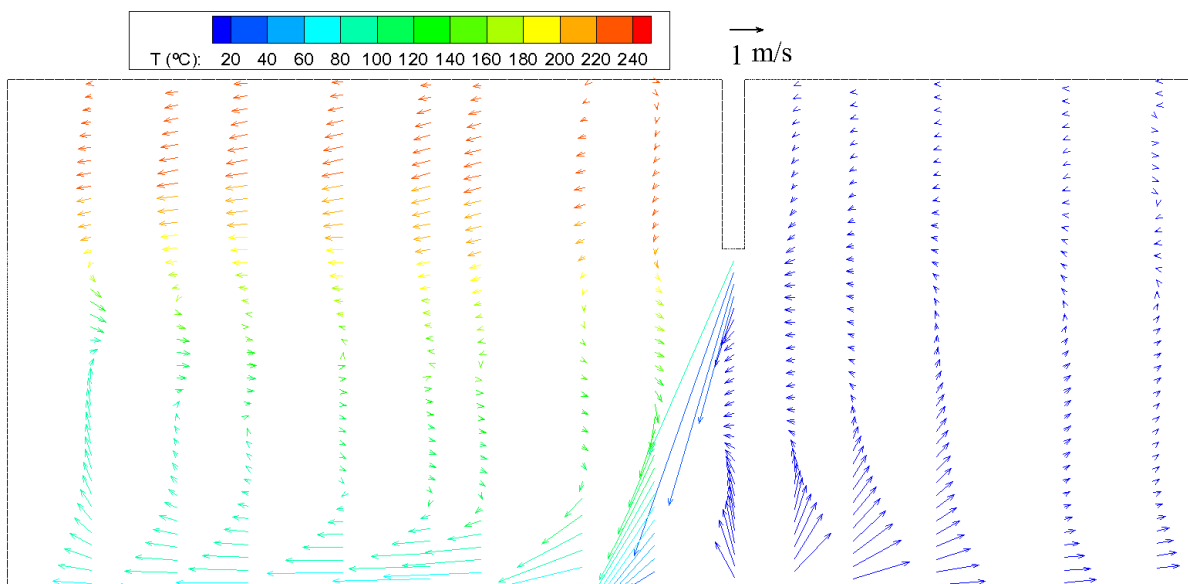
Figure 7: Velocity vector representing the flow with the active air curtain on the longitudinal section of the door.

Two different sets of simulations were performed to evaluate the influence of the efficiency of the air curtain on the exhaust flow rate. In the first set, the exhaust flow rate was calculated according to equation (5) and will be referred to as "½ nozzle". In the second set, the exhaust flow rate was calculated according to equation (6) and will be referred to as "½ nozzle + ½ jet". In this research, the exhaust flow rate, calculated in accordance with either equation (5) or (6), depends on the jet nozzle thickness and on the jet nozzle velocity.

$$\dot{V}_{exau\,st\_1/2\_nozzle} = 0.5\,\overline{u_0}wb_0 \tag{5}$$

$$\dot{V}_{exaust\_½\,nozzle\,+\,½\,jet} = \left[0.22\left(\frac{2x}{b_0}\right)^{0.5} + 0.5\right]\overline{u_0}wb_0 \tag{6}$$

In Table 1 the simulation reference number, the adopted exhaust flow rate and the Reynolds Number are presented in accordance with the characteristics of the jet. The theoretical rebuilding time of the air curtain after being crossed by a solid obstruction is also presented. Due to the high number of combinations of the studied variables, some possibilities were considered to be less important and were not simulated. The same table also presents the exhaust flow rate in the simulated combinations.

Table 1: Simulation characteristics.

Flow rate	Nozzle velocity [m/s]	Nozzle thickness [mm]	Curtain angle [°]			$\dot{V}_{exaust}$ [l/s]	$t_{rebuilding}$ [s]	Re
			10	**5**	**0**			
½ nozzle	1.0	25	N21b	-	N41b	11.3	3.7	1655.2
		10	N45	-	N40b	4.5	5.9	662.1

		5	N38b	-	N39b	2.3	8.3	331.0
		25	N24b	N28b	N42b	73.9	3.7	1655.2
½ jet + ½ nozzle		10	N25c	N29c	N37d	44.1	5.9	662.1
		5	N30d	N44d	N43c	30.3	8.3	331.0
	0.5	5	N35b	N36b	N33b	15.2	16.6	165.5

In this work, the air curtain efficiency is described by the ratio between the contamination aerodynamic sealing ability and the ideal case. This parameter $\boldsymbol{\eta}$, described by equation (7), is evaluated by the maximum contaminant concentration (C) in the adjacent plane of the door (out) and in the compartment (in). Variable C_{min} represents the minimum concentration in the field and had the value 0 for these simulations.

$$\eta = 1 - \frac{(C_{max})_{out} - C_{min}}{(C_{max})_{in} - C_{min}} \tag{7}$$

The results are presented in annex. Tables A.1 to A.3 show the results corresponding to the vertical cross section of the velocity field at the door symmetry plane. Tables A.4 to A.6 present the results corresponding to the vertical cross section of the concentration field of a passive scalar at the door symmetry plane. Tables A.7 to A.9 show the results corresponding to the vertical cross section of the concentration field of a passive scalar at the door front plane (this is the plane of the external surface of the wall containing the door). While in tables A.4 to A.6 the highest concentration of the passive scalar corresponds to 1, and hence, all contour lines have the same reference, in tables A.7 to A.9 the reference is different in each simulation case; the maximum contour color scale corresponding to the highest concentration of the passive scalar at the front door plane (shown at the top of the contour color scale).

Table 2 presents the maximum values of the concentration field of a passive scalar at the door front plane (this is the plane of the external surface of the wall containing the door). The same table shows that the maximum value of the contaminant concentration is 0.458, for vertical jets with a 25 mm thickness and a low exhaust flow rate ("½ nozzle"). Table 3 shows the air curtain efficiency parameter $\boldsymbol{\eta}$ for the same plane. It is observed that for vertical jets with different jet thicknesses, the contaminant concentration that flows to the outside of the compartment does not vary significantly with the thickness. This shows that the air curtain efficiency is almost independent of the jet thickness when the extraction flow rate is correlated with the jet thickness by equations (5) or (6).

Table 2: Contaminant concentration of a passive scalar.

Flow rate	Nozzle velocity [m/s]	Nozzle thickness [mm]	Curtain angle [°]			$\dot{V}_{exaust}$ [l/s]	$t_{rebuilding}$ [s]	Re
			10	5	0			
½ nozzle		25	0.254	-	0.458	11.3	3.7	1655.2
		10	0.298	-	0.432	4.5	5.9	662.1
	1.0	5	0.355	-	0.452	2.3	8.3	331.0
		25	0.013	0.020	0.184	73.9	3.7	1655.2
½ jet + ½ nozzle		10	0.010	0.009	0.098	44.1	5.9	662.1
		5	0.015	0.011	0.062	30.3	8.3	331.0
	0.5	5	0.083	0.062	0.051	15.2	16.6	165.5

Table 3: Sealing efficiency of the air curtain for different cases.

Flow rate	Nozzle velocity [m/s]	Nozzle thickness [mm]	Curtain angle [°]			$\dot{V}_{exaust}$ [l/s]	$t_{rebuilding}$ [s]	Re
			10	5	0			
½ nozzle		25	74.6	-	54.2	11.3	3.7	1655.2
		10	70.2	-	56.8	4.5	5.9	662.1
	1.0	5	64.5	-	54.8	2.3	8.3	331.0
		25	98.7	98.0	81.6	73.9	3.7	1655.2
½ jet + ½ nozzle		10	99.0	99.1	90.2	44.1	5.9	662.1
		5	98.5	98.9	93.8	30.3	8.3	331.0
	0.5	5	91.7	93.8	94.9	15.2	16.6	165.5

The following results were obtained:
- The analysis of the velocity field shows that the angle of the jet is important to define the flow path just near the nozzle. Far from the nozzle the flow path of the jet depends mainly on the extraction flow rate from

the compartment. In table A.1 the exhaust flow rate corresponds to just half of the nozzle flow rate; therefore, half of the jet flow rate is rejected to the outside; it can be seen that the jet near the floor impingement point is approximately vertical, both for the angle 0° and the angle 10°. In table A.2, the exhaust flow rate corresponds to the full jet flow rate; therefore, the jet is pushed into the compartment approximately in the same way for every jet angle (0°, 5° or 10°).

- Table A.1 shows that a significant part of the jet flow rate is rejected to the outside in the case of exhaust rates corresponding to half of the nozzle flow rate and table A.2 shows that the rejected jet flow rate to outside is quite small, when the exhaust rate corresponds to a full jet flow rate. However, table A.2 shows that, even when the exhaust flow rate corresponds to the "non-contaminated" flow rate incorporated in the jet, there are still some turbulent eddies that transport the mass flux from the jet to the outside ("non-contaminated" side). This behaviourcan be confirmed in the analysis of the passive scalar field, which shows that the passive scalar concentration is always above zero outside the compartment (near the jet impingement zone of the floor).

- When the increase in the jet nozzle thickness and in the jet nozzle velocity is compensated by the exhaust flow rate, the general pattern of the velocity field does not change (despite the obvious changes in the intensity of the field).

- Tables A.4 to A.6 show that the jet is able to clearly separate the "contaminated" side from the "non-contaminated" side. The cross contamination occurs mainly in the rejected part of the jet at the floor impingement zone. This conclusion shows that the key issue to avoid the cross contamination through the jet is to prevent the rejected jet mass to flow into the "non-contaminated" side at the floor impingement zone.

- Table A.7 to A.9 show that there are two main zones where the turbulent jet flow, contaminated by the entrainment from the "contaminated" side, is transporting contaminants through the outer door plane (the assessment plane): (i) the zone near the nozzle (see table A.8) and (ii) the zone near the floor impingement zone. It is possible to observe that the contamination transport though the outer door plane near the nozzle does not occur when the jet angle is 10° (see tables A.8 and A.9). Moreover, the exhaust flow rate from the "contaminated" compartment, as it deflects the jet it reduces the area with cross contamination near the nozzle (it is possible to compare the vertical jets shown in table A.7 with the vertical jets shown in tables A.8 and A.9). The main conclusion is that this contaminated zone near the nozzle corresponds to just a part of the jet turbulent flow but does not release a significant contamination to the "non-contaminated" side, because otherwise it would be possible to observe some contamination in this zone when the jet angle was 10°. This conclusion emphasizes the notion that the control of the cross contamination through the jet relies mainly on the behaviour at the floor impingement zone.

- Tables 2 and 3 show that the cross contamination decreases when the exhaust flow rate condition (from the "contaminated" compartment) increases (from equation 5 to 6). For the same flow rate condition (given by equations 5 or 6), and varying the jet nozzle thickness, there is no significant change in the air curtain efficiency η; this means that it is not influenced by the jet nozzle thickness (when the exhaust flow rate is correlated with the jet thickness). Moreover, the change in the jet angle from 5° to 10° does not have any significant impact on the air curtain efficiency η. The increase in the jet nozzle speed (from 0.5 m/s to 1.0 m/s and counterbalanced by the corresponding increase in the compartment exhaust rate) seems to have a small impact on the improvement of the air curtain efficiency η.

The rebuilding time of the air curtain (when an object or person cross it) was estimated and presented in Table 3. It ranged from 3.7 s to 16.6 s in the cases studied. The allowable rebuilding time will depend on the contaminant tightness requirements. If the required contaminant tightness is high the rebuilding time will supposedly be low. This research team considers that the rebuilding time of about 8 s is adequate for a number of applications. This requirement is compatible with the jet nozzle velocity of 1.0 m/s for a 2.0 m high air curtain.

IV. DISCUSSION

In a previous research carried out in the framework of this Nanoguard2ar research project [9], a small-scale water modelling allowed obtaining the empirical law presented in equation (8), which corresponds to the boundary of the contaminant tightness at the opening.

$$\overline{u_a} = \begin{cases} 0.0564 \times (1.00 - \sin\alpha_0) \ \times \overline{u_0}^{0.5} + 0.0026 & \text{if Re} \leq 1224 \\ 0.0564 \times \overline{u_0}^{0.5} + 0.0026 & \text{if Re} > 1224 \end{cases} \tag{8}$$

Moreover, the small scale water modeling experiments showed that:

- A velocity at the opening is still necessary to avoid the spread of the contamination when the jet is not active;

- There is no influence of the jet angle if $Re \geq 1710$;
- No influence of the nozzle thickness was observed in the experiments.

Using previous small-scale saltwater test results [4], the average velocity of the flow through the door, u_a , which is necessary to avoid the contaminant transport through the plane jet was related with the plane jet characteristics by equation (9). The comparison of the curves obtained with equations (8) and (9) (named "Prediction Ua" in the figure) is presented in figure 8 [9].

$$\overline{u_a} = 1.178 \times \left[0.22 \times \left(\frac{2 \times h}{b_0 \times \cos \alpha_0} \right)^{\frac{1}{2}} + 0.5 \right] \times \overline{u_0} \times \frac{b_0}{h} \tag{9}$$
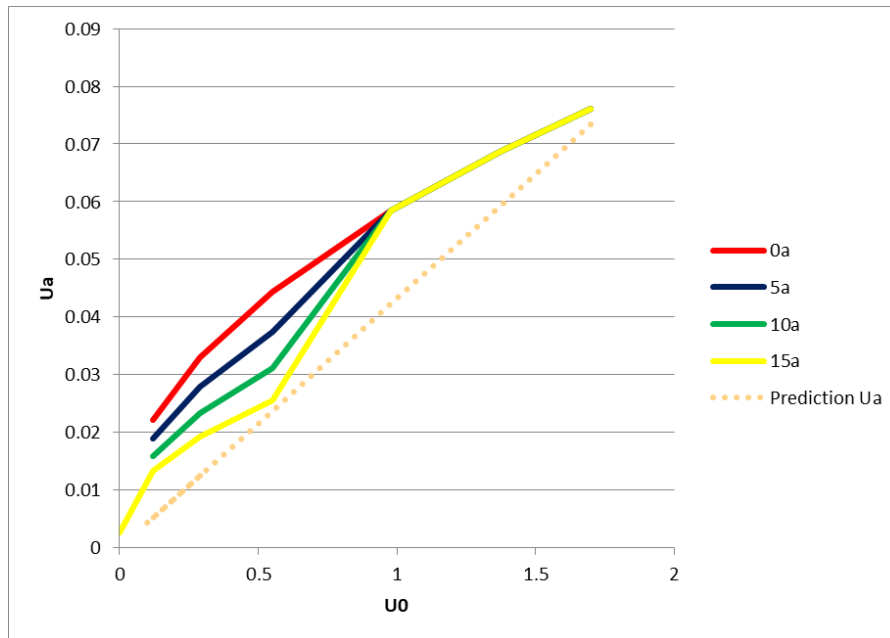

Figure 8: Comparison of equation (8) with the test results of equation (9) (Prediction Ua) [9]

A previous research project [37] analyzed the possibility of using air curtains to prevent smoke flow from fire compartments. Full size experiments were developed and several relevant conditions to assess aerodynamic sealing (smoke-tightness) were tested. The smoke temperature during the tests ranged from 182°C to 351°C, the angle measured between the curtain axis and the vertical plane ranged from 18° to 26°, the nozzle thickness ranged from 0.017 m to 0.045 m and the velocity at the nozzle ranged from 8.3 m/s to 19.9 m/s. During the tests, the air curtain's nozzle was positioned horizontally at the top outside edge of a permanent opening (door). With this configuration, we obtained an approximately vertical downward jet through the opening. It was concluded that it is possible to achieve an aerodynamic sealing (smoke-tightness), provided that the adequate plane jet parameters and the compartment's smoke exhaust are adjusted. According to this analysis, the smoke-tightness limit corresponds to equation $B = \Delta P_a / \Delta P_s = -0.30 \ \overline{u_a}/u_{a\_min} + 1.25$ (with $1.30 \leq \overline{u_a}/u_{a\_min} \leq 1.67)$, which allows relating the smoke exhaust flow rate with the nozzle air curtain velocity. A model for predicting the air curtain performance was also developed and validated with the experimental results. For that model $1.01 \leq \overline{u_a}/u_{a\_min} \leq 1.67$ and $B = \Delta P_a / \Delta P_s = -0.65 \ \overline{u_a}/u_{a\_min} + 2.04$ (see equation 11).

$$u_{a\_min} = \left[0,22 \times \left(\frac{2 \times h}{b_0 \times \cos \alpha_0} \right)^{\frac{1}{2}} + 0,5 \right] \times \overline{u_0} \times \frac{b_0}{h} \tag{10}$$

$$\overline{u_0} \geq \sqrt{\frac{B g h^2 \left(1 - \frac{T_0}{T_1} \right) - h \overline{u_a^2}}{b_0 \sin \alpha_0}} \tag{11}$$

Equation (10) has the same physical meaning as the one presented for equation (4) and equation (11) expresses the pressure balance at the door (the balance of the dynamic pressure of the jet, the dynamic pressure of the average velocity at the door and the smoke pressure). The aerodynamic sealing at the door should respect the two physical restrictions arising from these equations. T_0 and T_1 are, respectively, the absolute temperatures outside and inside the compartment. Variable g is the gravity acceleration.

Taking into account the definition of equation (10), it is evident that equation (9), obtained for salt water, expresses the same physical process, being $\overline{u_a}/u_{a\_min} = 1.178$.

It is clear now that the results obtained for small scale modeling, both in the saltwater modeling (representing a non-isothermal condition) and in the isothermal water modeling (without any density difference), can be used in a full size prototype. For both the Reynolds number Re > 1224 ($\overline{u_0} > 1.8\ m/s$ in figure 8) and the jet angle of 15°, equation (8) shows a similar development to equation (9) (but the dependence of $\overline{u_a}$ on $\overline{u_0}$ is not the same). Nonetheless, equation (8) requires a higher flow rate through the door, to reach the hydrodynamic sealing of the curtain, than the one predicted by equation (9) [9]. It is relevant to notice that even under such different test conditions (with or without buoyancy) a similar trend can be observed.

We admit also that the analytical model [37], obtained for high temperature differences (fire smoke control case), is still valid for low temperatures. According to that model, if $\overline{u_a}/u_{a\_min} = 1.178$, it will be possible to obtain $B = \Delta P_a / \Delta P_s = 1.27$. Furthermore, equation (8) can be expressed in terms of the Reynolds Number, as shown in equation (12). Following the same steps, equation (11) can also be expressed in terms of the Reynolds Number, as shown in equation (13).

$$u_a = \begin{cases} 0{,}0564 \times (1.00 - \sin \alpha_0) \quad \times \left(\frac{\text{Re} \times \mu}{\rho \times b_0}\right)^{0.5} + 0{,}0026 & \text{if Re} < 1224 \\ \\ \qquad 0{,}0564 \times \left(\frac{\text{Re} \times \mu}{\rho \times b_0}\right)^{0.5} + 0{,}0026 & \text{if Re} \geq 1224 \end{cases} \tag{12}$$

$$\text{Re} \geq \sqrt{\left[\frac{B\,g\,h^2\left(1 - \frac{T_0}{T_1}\right) - h\,\overline{u_a^2}}{b_0 \sin \alpha_0}\right]} \times \frac{\rho \times b_0}{\mu} \tag{13}$$

This later case is presented in figure 9. The dotted line ("Prediction Ua") corresponds to equation (9); this line is corresponding to the contaminant tightness in the isothermal flow. Above this line the exhaust flow rate is supercritical, and, then, an aerodynamic sealing (contaminant tightness) is obtained. The curved lines (named after the temperature difference between the exterior and the interior of the compartment) represent the limit of the aerodynamic sealing when a temperature difference exists (equation 13); in the direction of the graphic origin, the buoyancy flow driven is too strong and there is no aerodynamic sealing (loss of contaminant tightness). Equation 13 is presented in the graph for the particular case of $b_0 = 0.005$ m and h=0.66 m (the predicted location of the neutral plane below the door soffit; the door being 2 m high). This condition must be considered together with the condition obtained for the isothermal flow (equation 9). Therefore, it must be assumed that only the zone above the dotted line is relevant. The figure shows that, when there is a disturbance due to different temperatures inside and outside the compartment, the adoption of an air curtain (with the jet characterized by the Reynolds Number Re) allows reducing the average velocity through the door (Ua).

Figure 9 shows also the application of the equation (12), for a full-size air curtain prototype with $b_0 = 5$ mm. This graph shows clearly that only for the isothermal flow it is possible to avoid the contaminant transport through the opening by imposing a very low exhaust flow rate in the "contaminated" compartment ($\overline{u_a}$=0.0028 m/s). Even for a very small temperature difference (e.g., $\Delta T = T_1 - T_0$=0.5) the required exhaust flow rate in the "contaminated" compartment is higher with the air curtain inactive than with the air curtain active.

Figure 9 includes also the results of the simulations reported in section 3. For the curve named "½ nozzle", the exhaust flow rate of the simulations was calculated according to equation (5). For the curve named "½ nozzle + ½ jet", the exhaust flow rate of the simulations was calculated according to equation (6). The results corresponding to "½ nozzle" are very far from the tightness limit given by equations (9) and (12). The simulation results agree with this condition, showing that the tightness efficiency is between 54.2% and 74.6%. The results corresponding to "½ nozzle + ½ jet" are closer to the contaminant tightness limit given by equation (12) but still below the curves. The simulation results show that the tightness efficiency is between 90.2% and 99.1% and the higher efficiency values are obtained for higher jet angles. The simulation results are coherent with the experimental results. It is relevant to mention that the loss of aerodynamic sealing is not abrupt (decaying from 100% to 0%), when crossing the lines described by equations (9) and (12), but rather progressive. This opens the possibility of creating technical solutions, for cases where the required aerodynamic sealing is lower, by using lower exhaust flow rates.

Full size prototype tests are to be carried out afterwards to confirm the full analytical model.
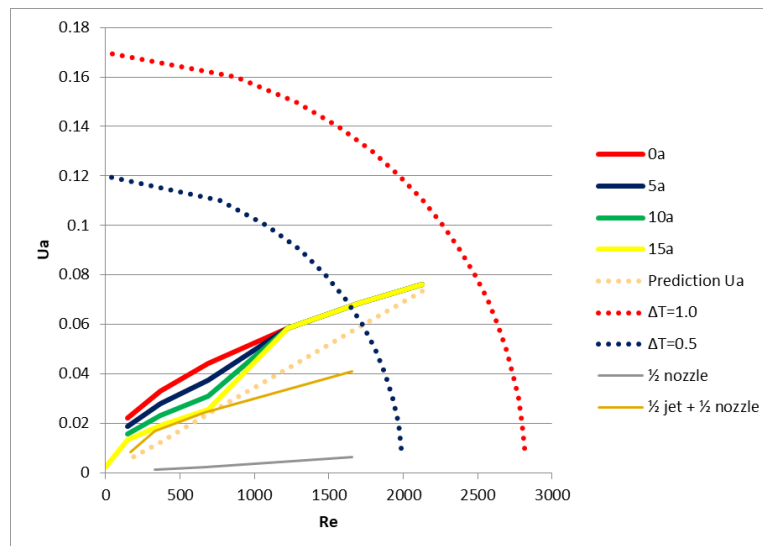
Figure 9: Prediction of air curtain contaminant tightness ($b_0 = 5$ mm) including simulation cases

V. CONCLUSIONS

In the works analysed in the State of the Art, there is no clear correlation between the inlet flow rate (flow entering the door opening) and the velocity at the jet nozzle, which ensures the maximum effectiveness of air curtains. The velocities normally assessed in these works were quite high and the Reynolds numbers adopted were higher than those adopted in our investigation. Therefore, to the best of the authors' knowledge, our research is innovative because explores the aerodynamic sealing performance for lower nozzle velocities.

The OpenFoam CFD code was validated for both the isothermal theoretical jets and the non-isothermal case of the air curtain and exhaust flow rate containing the contamination within a compartment. The OpenFoam computer code was used to investigate the case related with the "Air curtain isolating a 'contaminated' room".

The following results were obtained from the simulations:

- The analysis of the velocity field shows that the angle of the jet is important to define the flow path near the nozzle whereas, far from the nozzle, the flow path of the jet depends mainly on the extraction flow rate from the compartment.

- Simulation results show that the jet is able to clearly separate the "contaminated" side from the "non-contaminated" side. The cross contamination occurs mainly in the rejected part of the jet at the floor impingement zone. This conclusion shows that the key issue to avoid the cross contamination through the jet is to avoid the rejected jet mass flow rate to the "non-contaminated" side at the floor impingement zone.

- Simulation results show that there are two main zones where the turbulent jet flow, contaminated by the entrainment from the "contaminated" side, is transporting contaminant through the outer door plane (the assessment plane): (i) the zone near the nozzle and (ii) the zone near the floor impingement. However, the contaminated zone near the nozzle corresponds to just a part of the jet turbulent flow and no significant contamination is released to the "non-contaminated" side. This conclusion reinforces the notion that the control of the cross contamination through the jet relies mainly on the behaviour at the floor impingement zone.

- Simulation results show that the cross contamination decreases when the exhaust flow rate condition (from the "contaminated" compartment) increases (from equation 5 to 6). The air curtain efficiency η is not influenced by the jet nozzle thickness when the same flow rate condition (given by the equations 5 or 6) is kept. Moreover, the change in the jet angle from 5° to 10° does not demonstrate to have any significant impact on the air curtain efficiency η. The increase in the jet nozzle speed (from 0.5 m/s to 1.0 m/s) seems to have a small impact on the improvement of the air curtain efficiency η.

The air curtain rebuilding time (when an object or person crosses it) was estimated to range from 3.7 s to 16.6 s in the cases studied.

A review on experimental results previously obtained with saltwater modeling (small scale and representing a non-isothermal flow), water modeling (small scale and representing an isothermal flow) and a full size non-isothermal flow (fire situation), and compared with the simulation results reported in this research, shows that these results are coherent.

ACKNOWLEDGMENTS

NOMENCLATURE

b_0 – jet nozzle thickness [mm]

B - non-dimensional proportionality value assessed by experiments

C_{max} – maximum concentration of the contaminant

C_{min} - minimum concentration of the contaminant

C_{μ} - empirical constant specified in the turbulence model

D - diameter of the pool fire [m]

D_m - deflection modulus

g - gravity acceleration [m/s²]

h – door height [m], specific enthalpy [J/kg]

I - turbulence intensity [m/s]

k - turbulence kinetic energy [m²/s²]

K – scalar parameter

L_f - height of the flame [m]

$\dot{Q}$ - total heat release rate [W]

Re – Reynolds Number

s – passive scalar

$t_{rebuilding}$ - air curtain rebuilding time [s]

T – Temperature [K]

T_0 - absolute temperature outside the compartment [K]

T_1 - absolute temperature inside the compartment [K]

$\overline{u_0}$, u or U_0 – average jet nozzle velocity [m/s]

$\overline{u_a}$ – average velocity of the flow crossing the door [m/s]

u_{a_min} - minimum average velocity at the door given by equation (10) [m/s]

U(x,y) - longitudinal velocity of the jet [m/s]

$\dot{V}_{exaust}$ – exhaust flow rate [m³/s or l/s]

$\dot{V}_{exaust\_1/2\_nozzle}$ – exhaust flow rate corresponding to half of the jet nozzle flow rate [m³/s or l/s]

$\dot{V}_{exaust\_½\,nozzle\,+\,½\,jet}$ - exhaust flow rate corresponding to the flow rate of the jet supplied by the "non-contaminated" side [m³/s or l/s]

w – door width [m]

x –longitudinal coordinate of the jet [m]

X – jet length [m]

y - transversal coordinate of the jet [m]

α_0 – slope of the jet [°]

ΔP_s, - pressure difference due to the difference in fluid density between the interior and exterior [Pa]

ΔP_a - pressure difference due to momentum [Pa]

ε - turbulence kinetic energy dissipation rate [m²/s³]

η - air curtain efficiency

μ – fluid viscosity [Pa.s]

μ_t – turbulent viscosity [Pa.s]

ρ – fluid density [kg/m³]

REFERENCES

[1]. Garcia, H.G. Numerical Study and Experimental Optimization of air Curtains. Ph.D. Thesis, University Politècnica Catalunya, Barcelona, Spain, 2015.

[2]. Gonçalves, J.C.; Costa, J.J.; Figueiredo, A.R.; Lopes, A.M.G. CFD modelling of aerodynamic sealing by vertical and horizontal air curtains. *Energy Build*. 2012, 52, 153–160.

[3]. Costa, J.J.; Oliveira, L.A.; Silva, M.C.G. Energy savings by aerodynamic sealing with a downward-blowing plane air curtain—A numerical approach. *Energy Build*. 2006, 38, 1182–1193.

[4]. Viegas, J.C. Saltwater experiments with air curtains for smoke control in the event of fire. *J. Build. Eng*. 2016, 8, 243–248.

[5]. Krajewski, G. Efficiency of air curtains used for separating smoke free. In *Proceedings of the BS2013: 13th Conference of International Building Performance Simulation Association*, Chambéry, France, 26–28 August 2013.

[6]. Memarzadeh, F.; Jiang, J. Methodology for minimizing risk from airborne organisms in hospital isolation

rooms. *ASHRAE Trans*. 2000, 106.

[7]. Memarzadeh, F.; Manning, A. Comparison of Operating Room Ventilation Systems in the Protection of the Surgical Site. *ASHRAE J*. 2002, 108, 3–15.

[8]. Lim, T.; Cho, J.; Kim, B.S. Predictions and measurements of the stack effect on indoor airborne virus transmission in a high-rise hospital building. *Build. Environ*. 2011, 46, 2413–2424.

[9]. Viegas, J.C.; Oliveira, F.; Aelenei, D. Experimental Study on the Aerodynamic Sealing of Air Curtains. *Fluids* 2018, 3, 49;

[10]. Hayes, F.C. Heat Transfer Characteristics of the Air Curtain: A Plane Jet Subjected to Transverse Pressure and Temperature Gradients. Ph.D. Thesis, University of Illinois, Champaign, IL, USA, 1968.

[11]. Hayes, F.C.; Stoecker, W.F. Design data for air curtains. *ASHRAE Trans*. 1969, 75, 168–180.

[12]. Hayes, F.C.; Stoecker, W.F. Heat transfer characteristics of the air curtain. *ASHRAE Trans*. 1969, 75, 153–167.

[13]. Goubran, S.; Qi, D.; Saleh, W.; Wang, L.; Zmeureanu, R. Experimental study on the flow characteristics of air curtains at building entrances. *Build. Environ*. 2016, 105, 225–235.

[14]. Goubran, S.; Qi, D.; Wang, L. Assessing dynamic efficiency of air curtain in reducing whole building annual energy usage. *Build. Simul*. 2017, 10, 497–507.

[15]. Zhai, Z.J.; Osborne, A.L. Simulation-based feasibility study of improved air conditioning systems for hospital operating room. *Front. Archit. Res*. 2013, 2, 468–475.

[16]. Chow, T.T.; Yang, X.Y. Performance of ventilation system in a non-standard operating room. *Build. Environ*. 2003, 38, 1401–1411.

[17]. Cook, G.; Int-Hout, D. Air motion control in the Hospital Operating Room. *ASHRAE J*. 3(1):30–36 2009.

[18]. Shih, Y.C.; Yang, A.S.; Lu, C.W. Using air curtain to control pollutant spreading for emergency management in a cleanroom. *Build. Environ*. 2011, 46, 1104–1114.

[19]. Cook, G.; Int-Hout, D. A new idea that is 40 years old—Air curtain hospital operating room systems. *ASHRAE Trans*. 2007, 113, 349–357.

[20]. Swift, J.; Avis, E.; Millard, B.; Lawrence, T.M. Air Distribution Strategy Impact on Operating Room Infection Control. In *Proceedings of the Clima 2007*WellBeing Indoors, Helsinki, June 2007.

[21]. Hyvärinen, M.; Hagström, K.; Grönvall, I.; Hynynen, P. Reducing bartenders exposure to ETS by a local ventilation—Field evaluation of the solution. In *Proceedings of the Indoor Air 2002*, 9th International Conference on Indoor Air Quality and Climate, Montery, CA, USA, 30 June–5 July 2002; pp. 133–137.

[22]. Skistad, H. Efficient Ventilation: Displacement Ventilation and Air Curtain Zoning. Norway, 2011 pp. 1–17.

[23]. Luo, X.; Gu, Z.; Yu, C.; Ma, T.; Kase, K. Efficacy of an air curtain system for local pit environmental control for relic preservation in archaeology museums. Indoor *Built Environ*. 2016, 25, 29–40.

[24]. De Santoli, L.; Cumo, F.; Mariotti, M. Air curtain as a barrier against pollutants in cultural heritage: A case study. *Air Pollut*. XIV 2006, 1, 385–392.

[25]. Amin, M.; Navaz, H.K.; Dabiri, D.; Faramarzi, R. Air curtains of open refrigerated display cases revisited: A new technique for infiltration rate measurements. *WIT Trans. Eng. Sci*. 2008, 61, 179–190.

[26]. Traboulsi, S.R.; Hammoud, A.; Khalil, M.F. Effects of jet inclination angle and geometrical parameters on air curtain performance. *ASHRAE Trans*. 2009, 115, 617–629.

[27]. Loubière, K.; Pavageau, M. Educing coherent eddy structures in air curtain systems. *Lett. Appl. Microbiol*. 2005, 2705, 4–6.

[28]. Rydock, J.P.; Hestad, T.; Haugen, H.; Skaret, J.E. An Isothermal Air Curtain for Isolation of Smoking Areas in Restaurants; *Proceedings of ROOMVENT 2000* - Air Distribution in Rooms, Oxford, June 2000.

[29]. Lu, F.K.; Fernandes, J.E. Visualizing the Flow Induced by an Air Curtain over a Mannequin Using Stereo Particle Image Velocimetry. In *Proceedings of the ISFV13*—13th international Symposium on Flow Visualization, Nice, France, 1–4 July 2008; pp. 1–10.

[30]. Qi, D.; Goubran, S.; Wang, L.; Zmeureanu, R. Parametric study of air curtain door aerodynamics performance based on experiments and numerical simulations. *Build. Environ*. 2018, 129, 65–73.

[31]. Wang, L.; Zhong, Z. An approach to determine infiltration characteristics of building entrance equipped with air curtains. *Energy Build*. 2014, 75, 312–320.

[32]. Frank, D.; Linden, P.F. The effects of an opposing buoyancy force on the performance of an air curtain in the doorway of a building. *Energy Build*. 2015, 96, 20–29.

[33]. ANSYS, ANSYS FLUENT User's Guide – Release 14.0, ANSYS, Canonsburg, PA, 2011.

[34]. DOE. EnergyPlus. Engineering Reference. The Reference to EnergyPlus Calculations. US Department of Energy. 2010.

[35]. Cruz, H.; Viegas, J.C. On-site assessment of the discharge coefficient of open windows. *Energy Build*. 2016, 126, 463–476.

[36]. Uruba V., Turbulence Handbook for Experimental Fluid Mechanics Professionals, 2012.

[37]. Viegas J. C., Cruz, H. Air Curtains Combined with Smoke Exhaust for Smoke Control in Case of Fire: Full-Size Experiments. *Fire Technology*, 2018.

[38]. HeskestadG.. The SFPE Handbook of Fire Protection Engineering, 3rd ed., vol. 2.1, National Fire Protection Association. 2002.

[39]. Launder, B.E., Spalding, D.B. The numerical computation of turbulent flows. *Computer Methods in Applied Mechanics and Engineering*. 1974, 3 (2): 269–289. doi:10.1016/0045-7825(74)90029-2.

[40]. Versteeg, H. K., e Malalasekera, W.. An introduction to computational fluid dynamics: The finite volume method. Harlow, England: Pearson Education Ltd. 2007.

[41]. Warhaft Z., Passive scalars in turbulent flows, *Annu. Rev. Fluid Mech*. 2000. 32:203–240.

[42]. Blevins, R.D. Applied Fluid Dynamics Handbook; New York, Van Nostrand Reinhold: 1984.
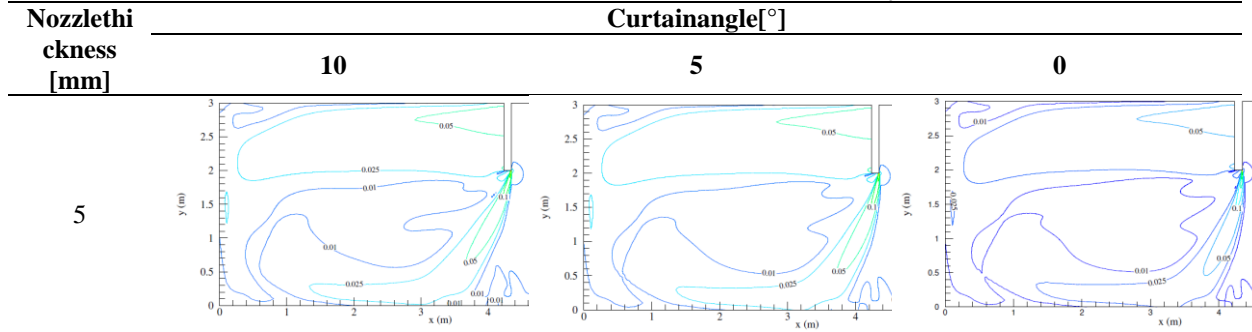
Annex – Simulation results

Table A.1: Vertical cross section of the velocity field at the door symmetry plane. Exhaust rate corresponding to ''½ nozzle'', $\overline{u_0}$=1.0 m/s

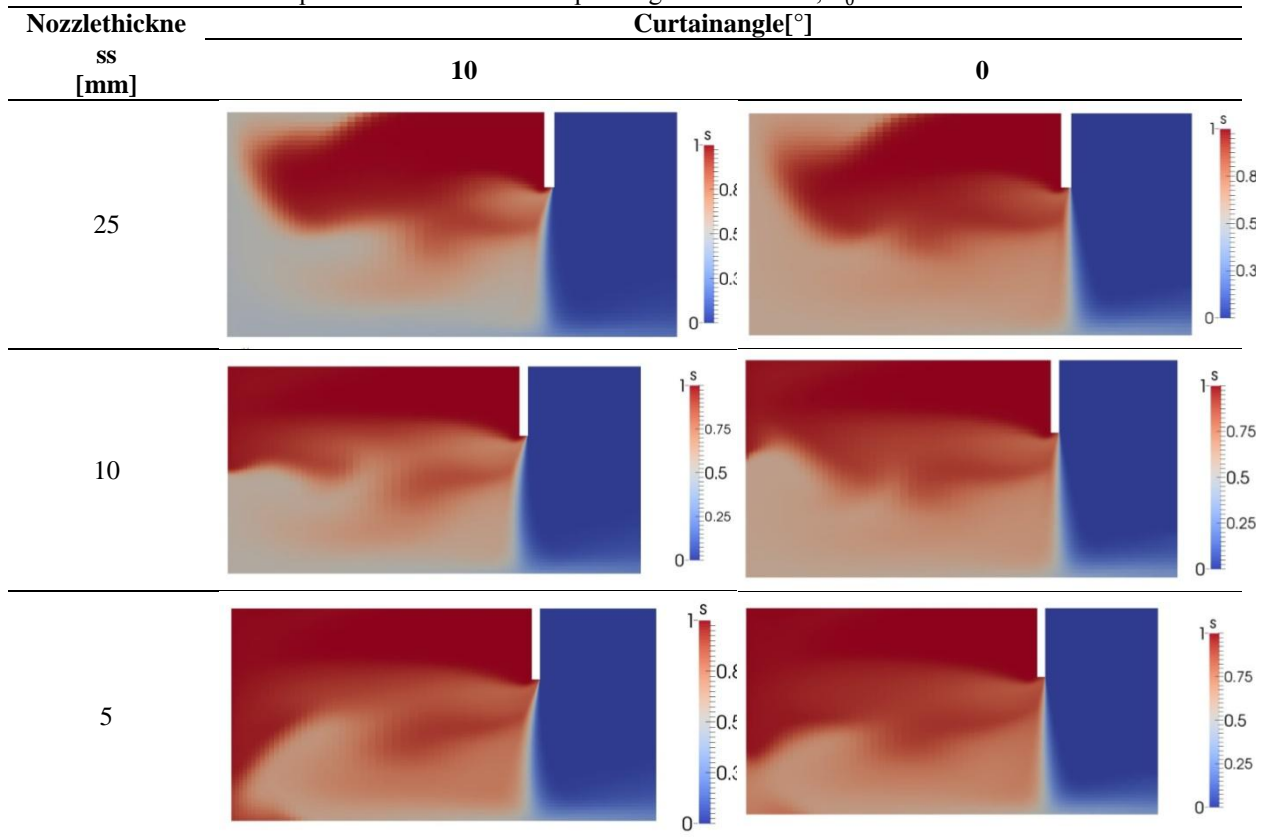| Nozzlethickness [mm]	Curtainangle[°]	
	10	**0**
25		
10		
5		
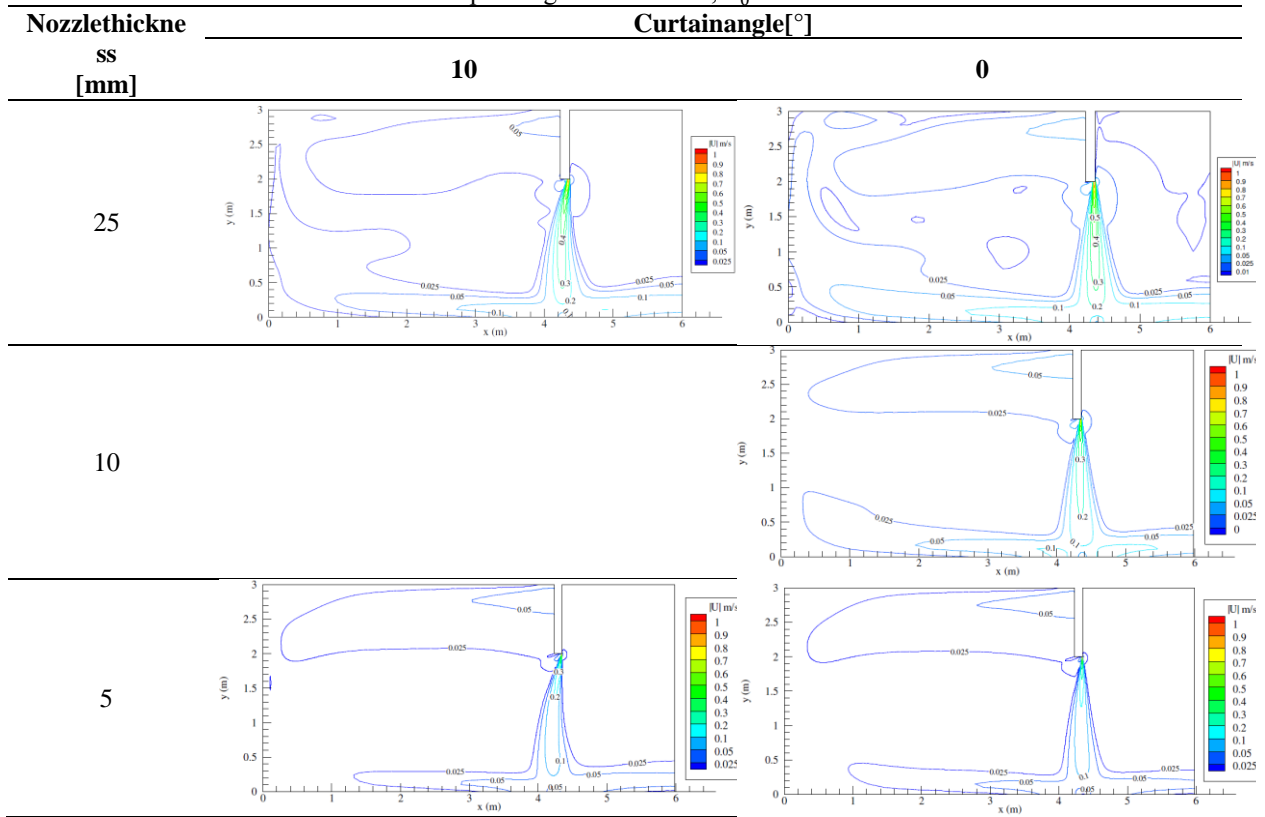
Table A.2: Vertical cross section of the velocity field at the door symmetry plane. Exhaust rate corresponding to ''½ nozzle + ½ jet'', $\overline{u_0}$=1.0 m/s

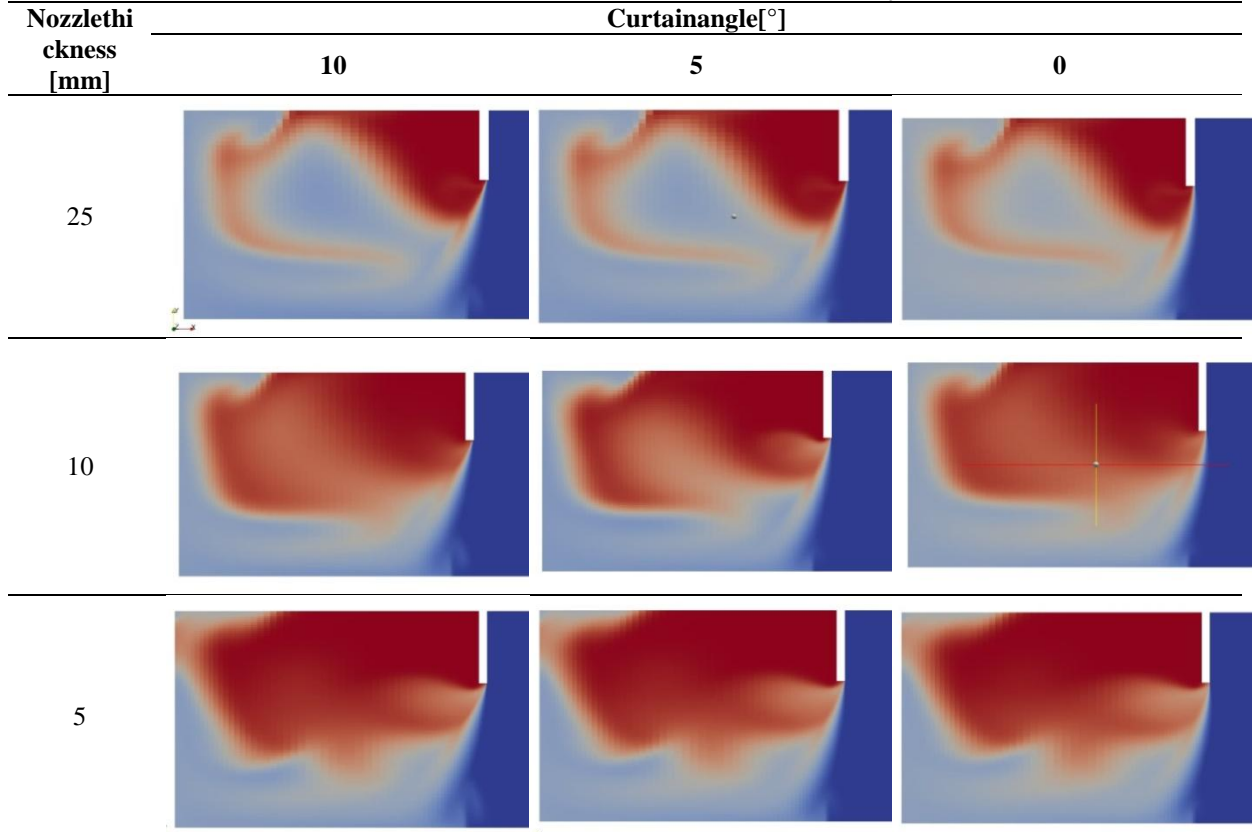| Nozzlethickness [mm]	Curtainangle[°]		
	10	**5**	**0**
25			
10			
5			
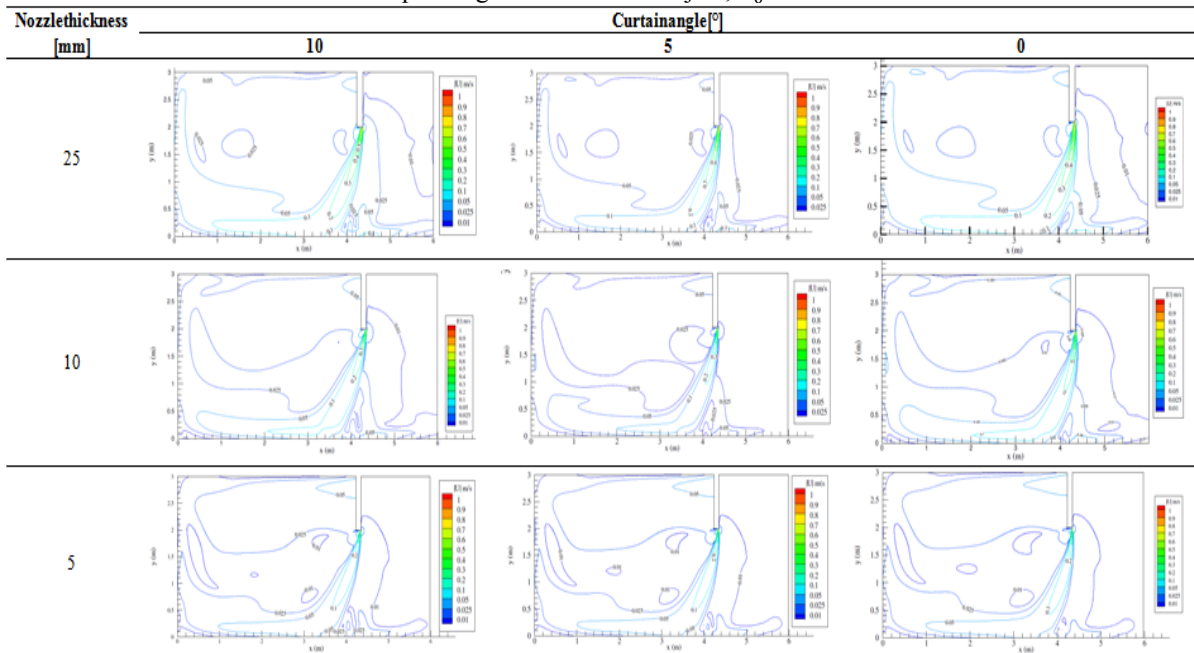
Table A.3: Vertical cross section of the concentration field of a passive scalar at the door symmetry plane. Exhaust rate corresponding to "½ nozzle + ½ jet", $\overline{u_0}$=0.5 m/s

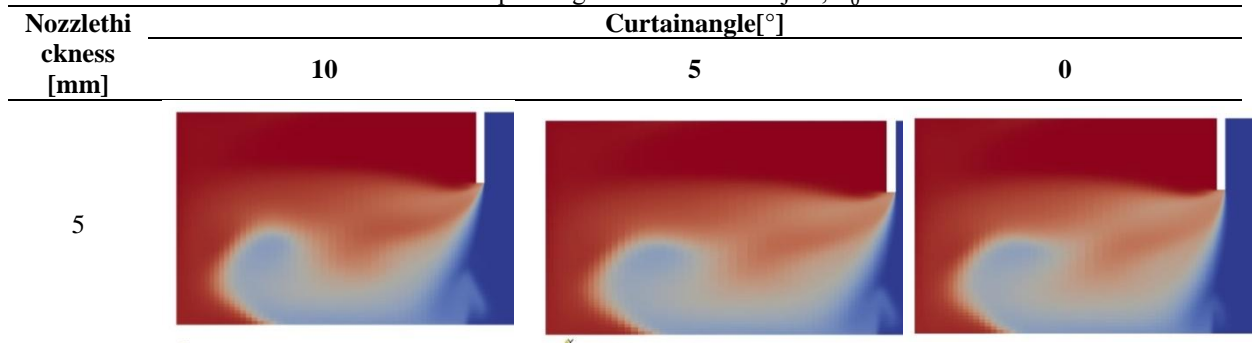| Nozzlethickness [mm]	Curtainangle[°]		
	10	**5**	**0**
5			

Table A.4: Vertical cross section of the concentration field of a passive scalar at the door symmetry plane. Exhaust rate corresponding to "½ nozzle", $\overline{u_0}$=1.0 m/s

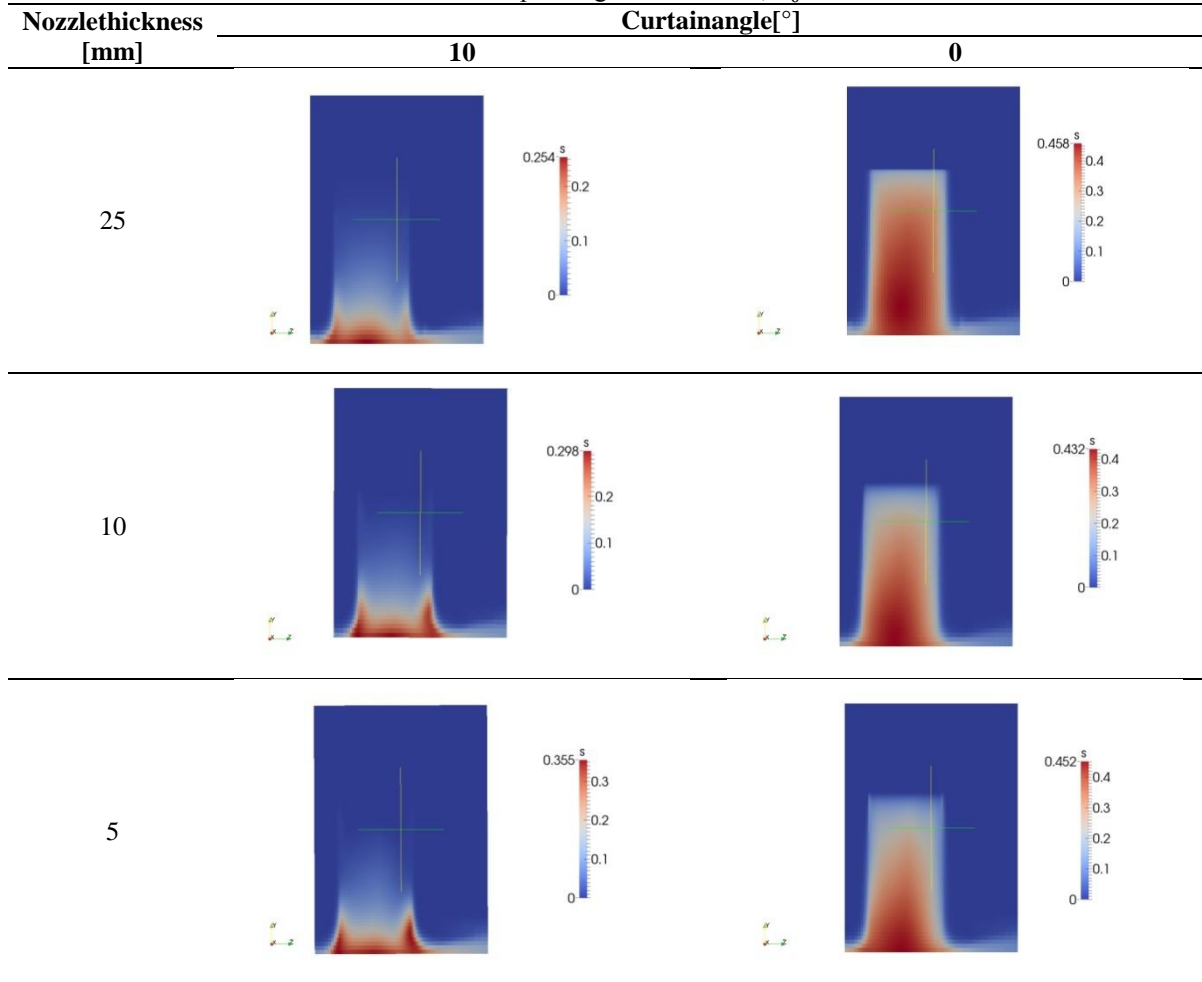| Nozzlethickness [mm]	Curtainangle[°]	
	10	**0**
25		
10		
5		

Table A.5: Vertical cross section of the concentration field of a passive scalar at the door symmetry plane. Exhaust rate corresponding to "½ nozzle + ½ jet", $\overline{u_0}$=1.0 m/s

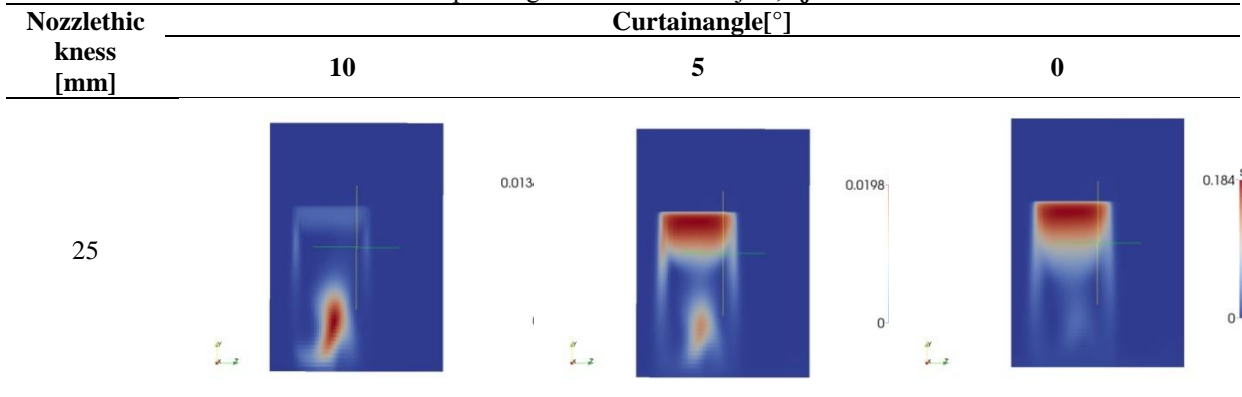| Nozzlethickness [mm]	Curtainangle[°]		
	10	**5**	**0**
25			
10			
5			

Table A.6: Vertical cross section of the concentration field of a passive scalar at the door symmetry plane. Exhaust rate corresponding to "½ nozzle + ½ jet", $\overline{u_0}$=0.5 m/s

Nozzlethickness [mm]	Curtainangle[°]		
	10	**5**	**0**
5			

Table A.7: Vertical cross section of the concentration field of a passive scalar at the door front plane. Exhaust rate corresponding to "½ nozzle", $\overline{u_0}$=1.0 m/s

Nozzlethickness [mm]	Curtainangle[°]	
	10	**0**
25		
10		
5		

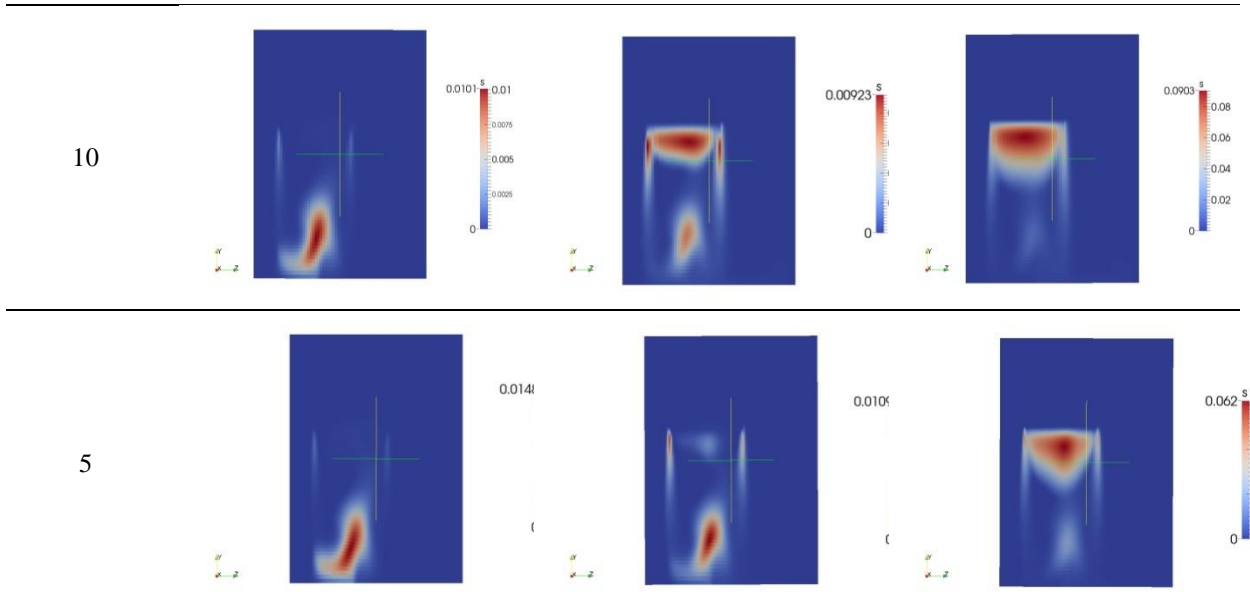

Table A.8: Vertical cross section of the concentration field of a passive scalar at the door front plane. Exhaust rate corresponding to "½ nozzle + ½ jet", $\overline{u_0}$=1.0 m/s

Nozzlethickness [mm]	Curtainangle[°]		
	10	**5**	**0**
25			

Table A.9: Vertical cross section of the concentration field of a passive scalar at the door front plane. Exhaust rate corresponding to "½ nozzle + ½ jet", $\overline{u_0}$=0.5 m/s

Nozzlethickness [mm]	Curtainangle[°]		
	10	**5**	**0**
5			

J. Dias. "CFD simulation of the aerodynamic sealing of plane jets." IOSR Journal of Engineering (IOSRJEN), vol. 09, no. 03, 2019, pp. 31-53.